

## Determining the local low-energy excitations in the Kondo semimetal CeRu<sub>4</sub>Sn<sub>6</sub> using resonant inelastic x-ray scattering

Andrea Amorese,<sup>1,2</sup> Kurt Kummer,<sup>3</sup> Nicholas B. Brookes,<sup>3</sup> Oliver Stockert,<sup>2</sup> Devashibhai T. Adroja,<sup>4,5</sup> André M. Strydom,<sup>5</sup> Andrey Sidorenko,<sup>6</sup> Hannes Winkler,<sup>6</sup> Diego A. Zocco,<sup>6</sup> Andrey Prokofiev,<sup>6</sup> Silke Paschen,<sup>6</sup> Maurits W. Haverkort,<sup>7</sup> Liu Hao Tjeng,<sup>2</sup> and Andrea Severing<sup>1,2</sup>

<sup>1</sup>*Institute of Physics II, University of Cologne, Zùlpicher Straße 77, D-50937 Cologne, Germany*

<sup>2</sup>*Max Planck Institute for Chemical Physics of Solids, Nöthnitzer Straße 40, D-01187 Dresden, Germany*

<sup>3</sup>*European Synchrotron Radiation Facility, 71 Avenue des Martyrs, CS40220, F-38043 Grenoble Cedex 9, France*

<sup>4</sup>*ISIS Facility, Rutherford Appleton Laboratory, Chilton, Didcot Oxon OX11 0QX, United Kingdom*

<sup>5</sup>*Highly Correlated Matter Research Group, Physics Department, University of Johannesburg,*

*P.O. Box 524, Auckland Park 2006, South Africa*

<sup>6</sup>*Institute of Solid State Physics, Vienna University of Technology, Wiedner Hauptstraße 8-10, A-1040 Vienna, Austria*

<sup>7</sup>*Institute for Theoretical Physics, Heidelberg University, Philosophenweg 19, D-69120 Heidelberg, Germany*



(Received 13 June 2018; revised manuscript received 10 August 2018; published 27 August 2018)

We have investigated the local low-energy excitations in CeRu<sub>4</sub>Sn<sub>6</sub>, a material discussed recently in the framework of strongly correlated Weyl semimetals, by means of Ce *M*<sub>5</sub> resonant inelastic x-ray scattering (RIXS). The availability of both <sup>2</sup>*F*<sub>5/2</sub> and <sup>2</sup>*F*<sub>7/2</sub> excitations of the Ce 4*f*<sup>1</sup> configuration in the spectra allows for the determination of the crystal-electric field (CEF) parameters that explain quantitatively the high-temperature anisotropy of the magnetic susceptibility. The absence of an azimuthal dependence in the spectra indicates that all CEF states are close to being rotational symmetric. We show further that the non-negligible impact of the  $\check{A}_6^0$  parameter on the ground state of CeRu<sub>4</sub>Sn<sub>6</sub> leads to a reduction of the magnetic moment  $\mu_c$  due to multiplet intermixing. This improves the agreement between CEF calculations and the experimentally determined magnetic susceptibility considerably at low temperatures. Deviations that persist at low temperatures for fields within the tetragonal plane are attributed to the Kondo interaction between 4*f* and conduction electrons. The RIXS results are consistent with inelastic neutron scattering data and are compared to the predictions from *ab initio* based electronic structure calculations.

DOI: [10.1103/PhysRevB.98.081116](https://doi.org/10.1103/PhysRevB.98.081116)

In several Ce compounds the localized 4*f* electrons hybridize with the conduction electrons (*cf* hybridization) so that hybridization gaps can form and give rise to Kondo insulating, semiconducting, or semimetallic ground states [1]. These materials are presently the focus of interest due to the proposal that the combination of strong spin-orbit coupling, bands of opposite parity (4*f* and 5*d*), plus the hybridization-induced gap should give rise to strongly correlated nontrivial topological phases [2–6]. CeRu<sub>4</sub>Sn<sub>6</sub> is a tetragonal, noncentrosymmetric (*I42m*) [7] compound. Its electrical resistivity increases as temperature decreases, which has been attributed to the opening of a hybridization gap of the order of 100 K [8–12]. The absence of magnetic order down to 50 mK [13] and the noninteger valence of 3.08 [14,15] confirm the importance of strong *cf* hybridization. Recently, band-structure calculations in the local density approximation (LDA)+Gutzwiller scheme have suggested that CeRu<sub>4</sub>Sn<sub>6</sub> is a correlated Weyl semimetal [16], a conjecture that remains to be tested experimentally, especially since the noncentrosymmetric crystal structure complicates the prediction for gap openings after a band inversion.

To understand the properties of CeRu<sub>4</sub>Sn<sub>6</sub> and to assess the reliability of the theoretical predictions we need to know not only the ground state but also the low-energy excitations of this system. The linear dichroism (LD) in soft x-ray

absorption (XAS) and the direction dependence in nonresonant inelastic scattering (NIXS) have shown that the crystal-electric field (CEF) ground-state symmetry must be the  $\Gamma_6$  [14], in agreement with magnetization measurements [10]. However, there is so far no information about the CEF level scheme, i.e., about the energy splittings  $\Delta E_1$  and  $\Delta E_2$  and the mixing factor  $\alpha$  of the excited CEF states. The present resonant inelastic x-ray scattering (RIXS) study aims at giving a full description of the CEF level scheme of CeRu<sub>4</sub>Sn<sub>6</sub>.

In an ionic model the trivalent (4*f*<sup>1</sup>) configuration of Ce is split by the effect of spin-orbit interaction ( $\approx 280$  meV) in two multiplets, <sup>2</sup>*F*<sub>5/2</sub> and <sup>2</sup>*F*<sub>7/2</sub>, with sixfold ( $J_z = \{-\frac{5}{2}; \dots; +\frac{5}{2}\}$ ) and eightfold degeneracy ( $J_z = \{-\frac{7}{2}; \dots; +\frac{7}{2}\}$ ). This degeneracy is further reduced by the interaction with the surrounding ions in the crystal and can be modeled with an effective CEF potential, written as a sum of (renormalized) spherical harmonics  $C_k^m = \sqrt{\frac{4\pi}{2k+1}} Y_k^m$ ,

$$V_{\text{CEF}}(r, \theta, \Phi) = \sum_{k=0}^{\infty} \sum_{m=-k}^k A_k^m r^k C_k^m(\theta, \Phi).$$

The expectation values  $\langle r^k \rangle$  cannot be calculated *ab initio* and are usually included in the phenomenological CEF parameters  $\check{A}_k^m = A_k^m \langle r^k \rangle$  that must be determined experimentally.

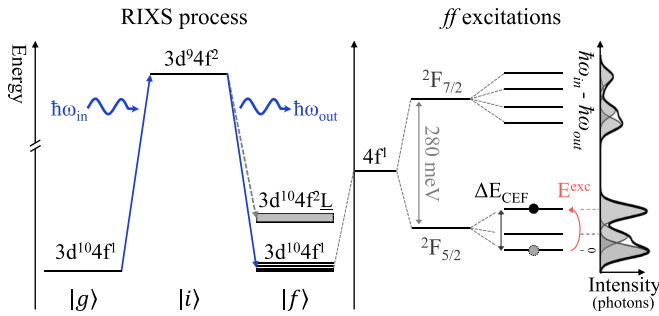


FIG. 1. Cerium  $M_{4,5}$ -edge RIXS process and  $ff$  excitations (see text).

Five independent parameters  $\check{A}_2^0$ ,  $\check{A}_4^0$ ,  $\check{A}_4^{\pm 4}$ ,  $\check{A}_6^0$ , and  $\check{A}_6^{\pm 4}$  fully describe the CEF problem for a  $\text{Ce}^{3+}$  ion with tetragonal point symmetry as in  $\text{CeRu}_4\text{Sn}_6$ . Nonzero  $\check{A}_4^{\pm 4}$  and  $\check{A}_6^{\pm 4}$  mix the  $J_z$  states according to  $\Delta J_z = 4$ , i.e.,  $J_z = \pm \frac{3}{2}$  and  $\mp \frac{5}{2}$ , and  $J_z = \pm \frac{1}{2}$  and  $\mp \frac{7}{2}$ , respectively. The intermixing of the two  $J$  multiplets  ${}^2F_{5/2}$  and  ${}^2F_{7/2}$  is usually negligible and the impact of the higher-order parameters  $\check{A}_6^0$  and  $\check{A}_6^{\pm 4}$  is small, even on the excited multiplet  ${}^2F_{7/2}$ , so that as a first approximation the three  $A_k^m$  parameters with  $k = 2$  and 4 describe the CEF problem. In this instance an analytical relationship can be given for the energy splittings of the ground-state multiplet, the mixing factor  $\alpha$ , and the CEF parameters (see Supplemental Material [17]). The three Kramers doublets of  ${}^2F_{5/2}$  can be written in the well-known  $|J, \pm J_z\rangle$  form as  $\Gamma_7^1 = \alpha | \frac{5}{2}; \pm \frac{5}{2} \rangle + \sqrt{1 - \alpha^2} | \frac{5}{2}; \mp \frac{3}{2} \rangle$ ,  $\Gamma_7^2 = \sqrt{1 - \alpha^2} | \frac{5}{2}; \pm \frac{5}{2} \rangle - \alpha | \frac{5}{2}; \mp \frac{3}{2} \rangle$ , and  $\Gamma_6 = | \frac{5}{2}; \pm \frac{1}{2} \rangle$ .

We apply high-resolution soft x-ray RIXS, an innovative spectroscopic technique, for determining the CEF level scheme of  $\text{CeRu}_4\text{Sn}_6$ . The first feasibility experiments have proven its sensitivity to  $ff$  excitations [18,19]. Following a second-order perturbation treatment, RIXS can be interpreted as the absorption of a photon resonant at a core edge of an ion in the system, followed by a reemission. When the system is left in an excited state, excitation energies are detected as energy losses of the scattered photons. This is depicted in Fig. 1 for the RIXS process at the Ce  $M_{4,5}$  edge ( $3d \rightarrow 4f$ ). From the ground state  $|g\rangle$  a  $3d$  electron is excited into the  $4f$  shell (intermediate state  $|i\rangle$ ) and then decays into the final state  $|f\rangle$  that can be the ground state (elastic scattering) or an excited state of the same configuration (magnons, phonons,  $ff$  excitations), or a different configuration via charge transfer [20–22]. Charge transfer excitations are usually broad and featureless compared to the (nearly) resolution-limited  $ff$  excitations and only contribute with a widely spread background, usually at higher-energy losses. We neither expect collective magnon nor phonon excitations in  $\text{CeRu}_4\text{Sn}_6$  due to the absence of magnetic order and the likely low electron-phonon coupling of the  $4f$  subshell. This is an effect of the resonant process, which imposes, in addition to element and valence selectivity, that all observable excitations must be coupled with the electronic levels involved in the RIXS process [23]. The strong resonance process ensures that the electronic excitations overwhelm dramatically (if not completely) the complex phonon background that usually is more visible in inelastic neutron scattering (INS) experiments. In addition, the very favorable signal-to-noise

ratio in comparison to INS and the ability to focus x rays allows measuring very small single crystals (surface  $\ll 1 \text{ mm}^2$ ).

Specific selection rules for polarization and scattering geometries provide further information about the magnetic versus charge origin of excitations, symmetry of the ground and excited states, and their orientation in the unit cell even in the presence of a higher than twofold rotational symmetry [19,24–27]. The latter is due to the fact that the selection rules in RIXS are  $\Delta J_z = 0, \pm 1, \pm 2$ , i.e., RIXS is not dipole limited as INS with  $\Delta J_z = 0, \pm 1$ . The RIXS spectrum should therefore provide a background-free mapping of the  $\text{Ce}^{3+}$   $4f$  energy levels, providing a direct measure the CEF splitting of both  ${}^2F_{5/2}$  and  ${}^2F_{7/2}$ , as depicted in Fig. 1.

$ff$  excitations are intra-atomic and well localized so that they can be simulated with a single ion full-multiplet calculation. Figure 2(a) shows the simulations of RIXS photon energy loss spectra at the Ce  $M_5$  edge for a single crystal, performed with the full-multiplet code QUANTY [28,29]. The atomic  $4f$ - $4f$  and  $4d$ - $4f$  Coulomb interactions were calculated with Cowan's atomic structure code [30]. Typical reductions of 20% and 30% [14,31] have been applied, respectively, to account for configuration interaction processes not included in the Hartree-Fock scheme [32]. The spin-orbit interaction in the  $4f$  shell has been reduced by 10% [18,19]. The calculations were set up for the backscattering geometry ( $2\theta = 150^\circ$ ), grazing incidence ( $\Theta^* = 20^\circ$ ), and with the tetragonal  $c$  axis (normal to the sample surface) in the scattering plane [see insets in Fig. 2(a)]. The calculations were carried out for the vertical polarization ( $\epsilon_v$ ) and two different sample orientations: blue lines for the  $[100]$  ( $\phi = 0^\circ$ ) and red lines for the  $[110]$  ( $\phi = 45^\circ$ ) in the scattering plane. The calculated intensities are convoluted with a 30-meV full width at half maximum (FWHM) Gaussian function representing the resolution achievable in experiments. The elastic intensity cannot be reliably calculated since surface roughness as well as low-energy collective excitations contribute to the (quasi)elastic signal. Instead, we show a resolution function of arbitrary height (gray lines centered at 0 meV).

The calculations in Fig. 2(a) are for a ground state with  $\Gamma_6$  symmetry [14] and for several mixing factors  $\alpha$  of the excited states at fixed energy splittings  $\Delta E_1$  and  $\Delta E_2$ .  $\alpha$  is defined such that the bottom curve ( $\alpha = 0$ ) refers to the sequence  $| \frac{5}{2}; \pm \frac{1}{2} \rangle$ ,  $| \frac{5}{2}; \pm \frac{3}{2} \rangle$ , and  $| \frac{5}{2}; \pm \frac{5}{2} \rangle$  for the ground, first, and second excited state. Accordingly,  $\alpha = 1$  resembles the sequence  $| \frac{5}{2}; \pm \frac{1}{2} \rangle$ ,  $| \frac{5}{2}; \pm \frac{5}{2} \rangle$ , and  $| \frac{5}{2}; \pm \frac{3}{2} \rangle$ . Figure S1 in the Supplemental Material shows calculations for different ground states and excited state sequences [17]. The calculations are based on only three parameters,  $\check{A}_2^0$ ,  $\check{A}_4^0$ , and  $\check{A}_4^{\pm 4}$ . Note that RIXS is sensitive to the orientation of the orbitals in the unit cell: Changing the sign of  $\check{A}_4^{\pm 4}$ , which is equivalent to changing the sign of  $\alpha$  in the calculation (not shown), causes a  $45^\circ$  rotation of the orbitals in the  $ab$  plane [33], and correspondingly inverts the  $\Phi$  dependence of the spectra (exchanges the blue and red lines).

The RIXS experiment on single-crystalline  $\text{CeRu}_4\text{Sn}_6$  [10,11,34] was performed at the ERIXS spectrometer of the ID32 beamline at ESRF, Grenoble, France with a resolution of 30 meV at the Ce  $M_5$  edge ( $\approx 880 \text{ eV}$ ) [19]. The inset of Fig. 2(b) shows the  $M$ -edge XAS spectra measured in the same geometry pointing out the incident photon energy

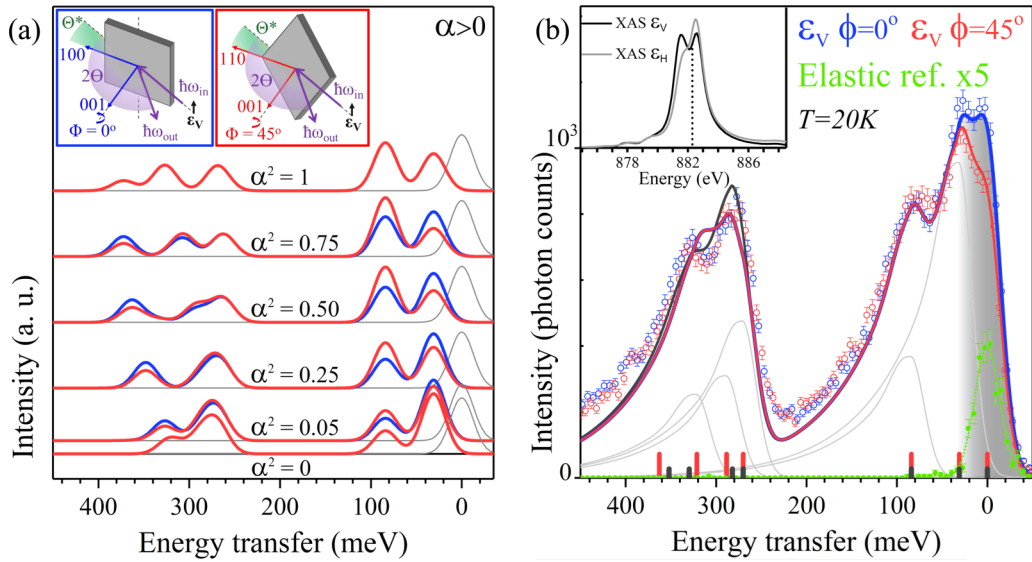


FIG. 2. (a) Calculated RIXS spectra at  $T = 20$  K as a function of the mixing parameter  $\alpha^2$  for  $\alpha > 0$ , with vertical polarization, for the two geometries  $\phi = 0^\circ$  and  $\phi = 45^\circ$  (see inset). (b) Experimental RIXS data (circles) with statistical error bars with the same scattering geometry as in the calculated RIXS spectra on the right. The red and blue lines (black line) show the full multiplet simulation with three (four) crystal-field parameters (the fourth being  $\check{A}_6^0 = 200$  meV) using an asymmetric line shape for the CEF excitations [see red (black) ticks and gray lines]. The respective CEF parameters are given in Table S1 in the Supplemental Material [17]. Note, the highest transition at  $\approx 360$  meV corresponds to a  $\Delta J_z = \pm 3$  transition and therefore has no spectral weight. The gray shading indicates the elastic region (see text). The elastic reference (green) shows the Gaussian response function of the beamline. XAS  $M_5$  edge and incident energy (dotted line) shown in the inset.

(882.2 eV) used for the RIXS spectroscopy. Figure 2(b) shows data for the two sample orientations  $\phi$  as in the calculation, i.e.,  $\phi = 0^\circ$  (blue dots) and  $\phi = 45^\circ$  (red dots). Both spectra have been acquired with incident vertical polarization. Other spectra acquired with different experimental settings can be found in Ref. [17]. The green dots are the measurements of carbon tape that serves as an elastic reference. More details of the beamline and setup can also be found in Ref. [17], which also contains Refs. [35,36].

The experimental RIXS spectra show two groups of peaks, the first one at 0–100 meV and the second at 250–400 meV, corresponding to the  ${}^2F_{5/2}$  multiplet and  ${}^2F_{7/2}$  multiplet, respectively. The spectra of both sample orientations show the expected three peaks in the  ${}^2F_{5/2}$  energy range: the elastic peak ( $E_0 = 0$  meV) plus two inelastic peaks at about  $\Delta E_1 \approx 30$  meV and  $\Delta E_2 \approx 85$  meV. In the  ${}^2F_{7/2}$  energy range we would expect to see four excitations due to the splitting into four Kramers doublets, however, while they are intense, they also seem to be too close in energy to be resolved.

The inelastic signals of the two experimental spectra are superimposed, reflecting no dependence on the rotation  $\phi$  around the  $c$  axis, thus suggesting the orbitals must have, or are close to, rotational symmetry which occurs in the presence of pure  $J_z$  states (see, e.g., Ref. [31]). Thus, the intermixing of  $J_z = \pm 3/2$  and  $\mp 5/2$  and of  $J_z = \pm 1/2$  and  $\mp 7/2$  of the excited states is next to zero, i.e.,  $\check{A}_4^{\pm 4}$  and also  $\check{A}_6^{\pm 4}$  must be negligibly small.

In the following we will compare the experimental data with calculations. The absence of a pronounced  $\phi$  dependence in the experiment [see Fig. 2(b)] indicates that  $\alpha$  is very close to 0 or 1 [see Fig. 2(a)]. Taking further into account the intensity ratios of the main peaks in either multiplet, we observe that the  $\alpha \approx 0$  calculation shows a better resemblance

to the experimental spectra. The only pronounced deviation in the experimental spectra between the two sample rotations is in the elastic region (see the gray shaded area). This could have either the trivial reason that the quality of the sample surface is different in the two positions, or it shows that  $\alpha$  is positive although close to zero [see Fig. 2(a)]. We can conclude that the excited CEF states of the lower multiplet are almost pure  $|J_z\rangle$  states with  $|\frac{5}{2}; \pm \frac{1}{2}\rangle$  being the ground state,  $|\frac{5}{2}; \pm \frac{3}{2}\rangle$  the first excited state, and  $|\frac{5}{2}; \pm \frac{5}{2}\rangle$  the second excited state.

Although we find a qualitative agreement between data and calculations, the overall spectral shapes differ. The calculation in Fig. 2(a) was performed with a Gaussian broadening resembling the resolution function, but the experimental spectral shapes are clearly non-Gaussian. Ignoring the non-Gaussian line shape could lead to larger energy transfers and/or unaccounted spectral weights [19]. We therefore used an empirical asymmetric line shape for the  $ff$  excitations (see Ref. [17]). The red (blue) line in Fig. 2(b) is the result of a calculation where each excitation is treated with the same asymmetric line shape and only the elastic peak is still convoluted with the Gaussian resolution function. We find the  $|\frac{5}{2}; \pm \frac{3}{2}\rangle$  state at  $\Delta E_1 = 31$  meV and the  $|\frac{5}{2}; \pm \frac{5}{2}\rangle$  at  $\Delta E_2 = 84$  meV with parameters  $\check{A}_2^0 = -163.7$  meV  $\check{A}_4^0 = -13.6$  meV, and  $\check{A}_4^4 = 0$  meV. Energies and excited state sequences of the  ${}^2F_{7/2}$  multiplet are given in Ref. [17]. The red ticks at the bottom scale denote the positions of the CEF excitations and the gray lines resemble the actual intensities. Note that in the calculation, the highest transition has zero intensity because it corresponds to a  $\Delta J_z = 3$  ( $|J_z = \pm \frac{1}{2}\rangle \rightarrow |J_z = \pm \frac{7}{2}\rangle$ ) transition which is not accessible due to selection rules. Also, spectra acquired with different experimental settings confirm the aforementioned results (see Ref. [17]).

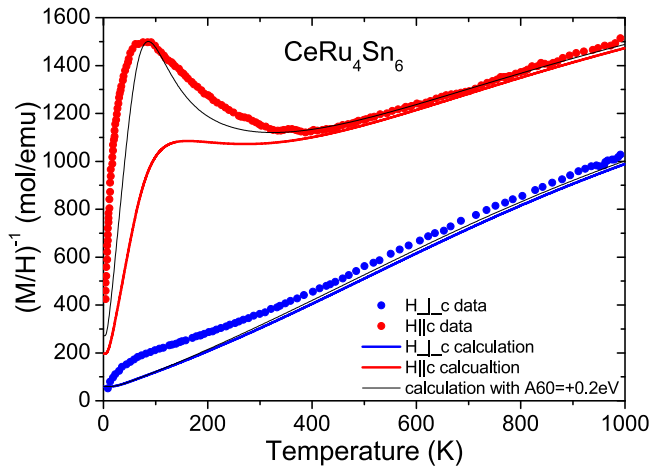


FIG. 3.  $(M/H)^{-1}$  curves of  $\text{CeRu}_4\text{Sn}_6$  measured with a 5- and 6-T magnetic field parallel (red dots) and perpendicular (blue dots) to the tetragonal  $c$  axis for  $T \leq 300$  K and  $T \geq 300$  K, respectively. The blue and red lines are the CEF-only calculation with  $\check{A}_6^0 = 0$  meV and the black lines with  $\check{A}_6^0 = 200$  meV.

Having determined the CEF parameters from the RIXS data, we now investigate to what extent these findings can explain the magnetic properties of the material. Figure 3 shows the experimental inverse magnetic susceptibility  $(M/H)^{-1}$  as a function of temperature for the magnetic field parallel (red dots) and perpendicular (blue dots) to the tetragonal  $c$  axis. We have calculated  $(M/H)^{-1}$  using the CEF parameters extracted from the RIXS experiment and plotted the results also in Fig. 3, for magnetic fields parallel (red lines) and perpendicular (blue lines) to the  $c$  axis. This three-parameter CEF model reproduces  $(M/H)^{-1}$  very well at temperatures above 400 K.

We now consider the higher-order parameters  $\check{A}_6^0$  and  $\check{A}_6^4$ . As stated above,  $\check{A}_6^4$  must be, as  $\check{A}_4^4$ , close to zero. Introducing a positive nonzero  $\check{A}_6^0$  leads to an increase in the peak intensity ratio in the energy range of the  ${}^2F_{7/2}$  multiplet. The black line and black ticks in Fig. 2(b) are the result of a calculation with  $\check{A}_6^0 = 200$  meV.  $\check{A}_6^0$  does not affect the high-temperature anisotropy of  $(M/H)^{-1}$  but improves the agreement of CEF-only calculation and data for fields parallel  $c$  at low temperatures (see the black lines in Fig. 3). The nonzero  $\check{A}_6^0$  increases the multiplet intermixing so that the new ground-state wave function |GS) now contains a considerable amount of the  ${}^2F_{7/2}$  multiplet,

$$|GS) = 0.99|J = 5/2, J_z = \pm \frac{1}{2}\rangle + 0.12|J = 7/2, J_z = \pm \frac{1}{2}\rangle.$$

This goes along with a reduction of the magnetic moment  $\mu_{\parallel c}$  from  $0.45\mu_B$  to  $0.33\mu_B$  as calculated from the CEF model. The further impact of  $\check{A}_6^0$  on the excited states is listed in Table S1 in Ref. [17]. On the contrary,  $(M/H)^{-1}_{H\perp c}$  (blue dots) is unaffected by  $\check{A}_6^0$  and we attribute its deviation from the CEF-only calculation for  $T < 400$  K to the Kondo effect [12].

The classical tool for determining the CEF scheme in rare-earth compounds is INS so that compatibility of RIXS and INS data is essential. Figure 4 shows time-of-flight INS data of polycrystalline  $\text{CeRu}_4\text{Sn}_6$  on an absolute intensity scale. Polycrystalline  $\text{LaRu}_4\text{Sn}_6$  was measured as a nonmagnetic

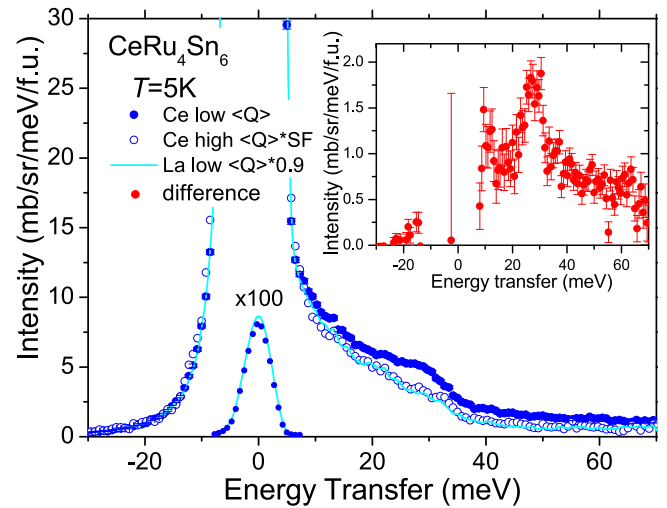


FIG. 4. Inelastic neutron scattering (INS) data at 5 K of  $\text{CeRu}_4\text{Sn}_6$  (blue dots) at low momentum transfers ( $\langle Q \rangle = 2.2 \text{ \AA}^{-1}$ ) compared to the nuclear scattering of high to low  $\langle Q \rangle$  scaled  $\text{CeRu}_4\text{Sn}_6$  (open dots) and nonmagnetic scattering-length corrected low  $\langle Q \rangle$   $\text{LaRu}_4\text{Sn}_6$  (cyan line) (see Supplemental Material [17]). The strong elastic scattering has been divided by a factor of 100. Inset: Magnetic scattering as determined from the difference of low  $\langle Q \rangle$   $\text{CeRu}_4\text{Sn}_6$  and high to low  $\langle Q \rangle$  scaled  $\text{CeRu}_4\text{Sn}_6$  nuclear scattering. All data are normalized to absolute intensities.

reference compound. The low angle data are grouped for low momentum transfers  $\langle Q \rangle = 2.2 \text{ \AA}^{-1}$  where the magnetic form factor is large. The spectra contain incoherent nuclear elastic and inelastic (phonon) scattering as well as, in the case of Ce, incoherent magnetic scattering (see the solid blue dots). To extract the magnetic scattering, the nuclear contribution has been assigned by high to low  $\langle Q \rangle$  scaling (open dots) and scaling of the nonmagnetic reference data (cyan line). More experimental details as well as explanations of the phonon correction are given in Ref. [17]. The difference of the solid and open dots yields the magnetic scattering (see inset). There is a clear peak at about 30 meV in agreement with RIXS. Its magnetic origin has been further confirmed by comparing the Ce and La data at large momentum transfers [see Fig. S3(a) in Ref. [17]]. The second CEF excitation at 80–85 meV is not only outside the energy window of the present INS experiment, but it is also dipole forbidden ( $\Delta J_z = \pm 2$ ), i.e., not observable in an INS experiment. The integrated intensity of the excitation at 30 meV is compatible with the CEF model that describes the RIXS data, at 5 K as well as at 300 K (see Ref. [17]). It is important to mention that high-resolution INS data (not shown) confirm the absence of any lower-lying CEF excitation.

We now compare the RIXS and INS results with electronic structure calculations. Wissgott *et al.* [37] performed density functional theory (DFT) plus dynamical mean-field theory (DMFT) calculations of  $\text{CeRu}_4\text{Sn}_6$  for treating the strong correlation effects of  $f$  electrons of Ce and find a  $|\frac{5}{2}; \pm \frac{1}{2}\rangle$  ground state with some mixing of the higher multiplet  ${}^2F_{7/2}$  and with some contribution of  $|\frac{5}{2}; \pm \frac{3}{2}\rangle$  due to  $cf$  hybridization. Xu *et al.* [16] performed LDA+Gutzwiller calculations and find the same CEF ground state as Wissgott *et al.*, but a stronger

contribution of  $|\frac{5}{2}; \pm\frac{5}{2}\rangle$  than  $|\frac{5}{2}; \pm\frac{3}{2}\rangle$  mixed in by hybridization. In RIXS, we find the  $|\frac{5}{2}; \pm\frac{3}{2}\rangle$  state at about 30 meV and the  $|\frac{5}{2}; \pm\frac{5}{2}\rangle$  above 80 meV. Hence, the Wissgott *et al.* scenario seems to be closer to the experiment.

In NIXS and XAS hybridization effects were seen in the reduction of the ground-state dichroism [14]. In RIXS, it should show in a modified elastic or quasielastic signal, but in the elastic region RIXS is resolution limited and also hampered by surface effects. However, the strongly asymmetric line shape in the RIXS spectra is attributed to the strong *cf* hybridization. We rule out that phonons are responsible for the line shape because the CEF excitations in the RIXS spectra of antiferromagnetic CeRh<sub>2</sub>Si<sub>2</sub> [19], a material with a much lower Kondo temperature, are resolution limited (30 meV Gaussian at FWHM). In CeRu<sub>4</sub>Sn<sub>6</sub> the excitations are in total 65 meV wide (FWHM): 15 meV Gaussian resolution limited on the low-energy side and more than twice as much on the high-energy side [see the gray lines in Fig. 2(b) and Eq. (1) in Ref. [17]]. We therefore believe the decay into the continuum due to the 4*f*-band hybridization, that is also responsible for the Kondo-like physics in this material, leads to these strongly asymmetric line shapes. Presently, these effects cannot be

calculated quantitatively, so that in the analysis the line shape had to be treated empirically.

In summary, the soft RIXS study of CeRu<sub>4</sub>Sn<sub>6</sub> yields a CEF potential with a  $\Gamma_6$  ground state and  $\Gamma_7$  states at about 30 and 85 meV with a mixing factor  $\alpha \approx 0$  that reproduces the high-temperature anisotropy of  $(M/H)^{-1}$ ; no adjustment of energy transfers or mixing parameters was required to obtain the excellent agreement. The introduction of the higher-order CEF parameter  $\check{A}_6^0$  even reproduces the peak in  $M/H^{-1}$  at about 60 K for fields parallel to *c* by reducing the magnetic moment  $\mu_{\parallel c}$  of the ground state via intermultiplet mixing. It might well be that here the *J* mixing mimics to some extent the reduction of the ground-state moment due to the presence of strong *cf* hybridization. The latter shows up in the RIXS spectra as a strongly asymmetric line shape.

A.A. and A.S. benefited from financial support of the Deutsche Forschungsgemeinschaft through Grant No. SE1441/4-1. A.P., H.W., A.A.S., D.A.Z., and S.P. acknowledge financial support from the Austrian Science Fund (FWF I2535-N27) and S. Stojanovic for assistance in the sample preparation. A.M.S. thanks the SA NRF (93549) and the URC/FRC of UJ.

- 
- [1] P. S. Riseborough, *Adv. Phys.* **49**, 257 (2000).
- [2] M. Dzero, K. Sun, V. Galitski, and P. Coleman, *Phys. Rev. Lett.* **104**, 106408 (2010).
- [3] T. Takimoto, *J. Phys. Soc. Jpn.* **80**, 123710 (2011).
- [4] M. Dzero, J. Xia, V. Galitski, and P. Coleman, *Annu. Rev. Condens. Matter Phys.* **7**, 249 (2016).
- [5] S. Dzsaber, L. Prochaska, A. Sidorenko, G. Eguchi, R. Svagera, M. Waas, A. Prokofiev, Q. Si, and S. Paschen, *Phys. Rev. Lett.* **118**, 246601 (2017).
- [6] H.-H. Lai, S. E. Grefe, S. Paschen, and Q. Si, *Proc. Natl. Acad. Sci. U.S.A.* **115**, 93 (2018).
- [7] R. Pöttgen, R.-D. Hoffman, E. V. Sampathkumar, I. Das, B. D. Mosel, and R. Müllmann, *J. Solid State Chem.* **134**, 326 (1997).
- [8] I. Das and E. V. Sampathkumar, *Phys. Rev. B* **46**, 4250 (1992).
- [9] A. M. Strydom, Z. Guo, S. Paschen, R. Viennois, and F. Steglich, *Physica B* **359-361**, 293 (2005).
- [10] S. Paschen, H. Winkler, T. Nezu, M. Kriegisch, G. Hilscher, J. Custers, A. Prokofiev, and A. Strydom, *J. Phys.: Conf. Ser.* **200**, 012156 (2010).
- [11] H. Winkler, K.-A. Lorenzer, A. Prokofiev, and S. Paschen, *J. Phys.: Conf. Ser.* **391**, 012077 (2012).
- [12] V. Guritanu, P. Wissgott, T. Weig, H. Winkler, J. Sichelschmidt, M. Scheffler, A. Prokofiev, S. Kimura, T. Iizuka, A. M. Strydom, M. Dressel, F. Steglich, K. Held, and S. Paschen, *Phys. Rev. B* **87**, 115129 (2013).
- [13] A. M. Strydom, A. D. Hillier, D. T. Adroja, S. Paschen, and F. Steglich, *J. Magn. Magn. Mater.* **310**, 377 (2007).
- [14] M. Sundermann, F. Strigari, T. Willers, H. Winkler, A. Prokofiev, J. M. Ablett, J.-P. Rueff, D. Schmitz, E. Weschke, M. M. Sala, A. Al-Zein, A. Tanaka, M. W. Haverkort, D. Kasinathan, L. H. Tjeng, S. Paschen, and A. Severing, *Sci. Rep.* **5**, 17937 (2015).
- [15] M. Sundermann, K. Chen, Y. Utsumi, Y.-H. Wu, K.-D. Tsuei, J. Haenel, A. Prokofiev, S. Paschen, A. Tanaka, L. H. Tjeng, and A. Severing, *J. Phys.: Conf. Ser.* **807**, 022001 (2017).
- [16] Y. Xu, C. Yue, H. Weng, and X. Dai, *Phys. Rev. X* **7**, 011027 (2017).
- [17] See Supplemental Material at <http://link.aps.org/supplemental/10.1103/PhysRevB.98.081116> for further RIXS calculations and spectra, experimental setup of RIXS and INS, line shape in RIXS, CEF wave functions, relation of CEF parameters, and  $\Delta E_i$  and  $\alpha$ .
- [18] A. Amorese, G. Dellea, M. Fanciulli, S. Seiro, C. Geibel, C. Krellner, I. P. Makarova, L. Braicovich, G. Ghiringhelli, D. V. Vyalikh, N. B. Brookes, and K. Kummer, *Phys. Rev. B* **93**, 165134 (2016).
- [19] N. B. Brookes, F. Yakhov-Harris, K. Kummer, A. Fondacaro, J. C. Cezar, D. Betto, E. Velez-Fort, A. Amorese, G. Ghiringhelli, L. Braicovich, R. Barrett, G. Berruyer, F. Cianciosi, L. Eybert, P. Marion, P. van der Linden, L. Zhang, *NIM A* **903**, 175 (2018).
- [20] M. Nakazawa, S. Tanaka, T. Uozumi, and A. Kotani, *J. Phys. Soc. Jpn.* **65**, 2303 (1996).
- [21] S. M. Butorin, D. C. Mancini, J.-H. Guo, N. Wassdahl, J. Nordgren, M. Nakazawa, S. Tanaka, T. Uozumi, A. Kotani, Y. Ma, K. E. Myano, B. A. Karlin, and D. K. Shuh, *Phys. Rev. Lett.* **77**, 574 (1996).
- [22] C. Dallera, K. Giarda, G. Ghiringhelli, A. Tagliaferri, L. Braicovich, and N. B. Brookes, *Phys. Rev. B* **64**, 153104 (2001).
- [23] L. J. P. Ament, M. van Veenendaal, and J. van den Brink, *Europhys. Lett.* **95**, 27008 (2011).
- [24] L. Braicovich, M. Moretti Sala, L. J. P. Ament, V. Bisogni, M. Minola, G. Balestrino, D. Di Castro, G. M. De Luca, M. Salluzzo, G. Ghiringhelli, and J. van den Brink, *Phys. Rev. B* **81**, 174533 (2010).
- [25] M. M. Sala, V. Bisogni, C. Aruta, G. Balestrino, H. Berger, N. B. Brookes, G. M. de Luca, D. D. Castro, M. Grioni, M. Guarise, P. G. Medaglia, F. M. Granozio, M. Minola, P. Perna, M. Radovic, M. Salluzzo, T. Schmitt, K. J. Zhou, L. Braicovich, and G. Ghiringhelli, *New J. Phys.* **13**, 043026 (2011).

- [26] M. Minola, G. Dellea, H. Gretarsson, Y. Y. Peng, Y. Lu, J. Porras, T. Loew, F. Yakhou, N. B. Brookes, Y. B. Huang, J. Pellicciari, T. Schmitt, G. Ghiringhelli, B. Keimer, L. Braicovich, and M. Le Tacon, *Phys. Rev. Lett.* **114**, 217003 (2015).
- [27] L. Braicovich, M. Minola, G. Dellea, M. L. Tacon, M. M. Sala, C. Morawe, J.-C. Peffen, R. Supruangnet, F. Yakhou, G. Ghiringhelli, and N. B. Brookes, *Rev. Sci. Instrum.* **85**, 115104 (2014).
- [28] M. W. Haverkort, *J. Phys.: Conf. Ser.* **712**, 012001 (2016).
- [29] M. W. Haverkort, M. Zwierzycki, and O. K. Andersen, *Phys. Rev. B* **85**, 165113 (2012).
- [30] R. D. Cowan, *The Theory of Atomic Structure and Spectra* (University of California Press, Berkeley, 1981).
- [31] P. Hansmann, A. Severing, Z. Hu, M. W. Haverkort, C. F. Chang, S. Klein, A. Tanaka, H. H. Hsieh, H.-J. Lin, C. T. Chen, B. Fåk, P. Lejay, and L. H. Tjeng, *Phys. Rev. Lett.* **100**, 066405 (2008).
- [32] A. Tanaka and T. Jo, *J Phys. Soc. Jpn.* **63**, 2788 (1994).
- [33] T. Willers, F. Strigari, N. Hiraoka, Y. Q. Cai, M. W. Haverkort, K.-D. Tsuei, Y. F. Liao, S. Seiro, C. Geibel, F. Steglich, L. H. Tjeng, and A. Severing, *Phys. Rev. Lett.* **109**, 046401 (2012).
- [34] A. Prokofiev and S. Paschen, in *Modern Aspects of Bulk Crystal and Thin Film Preparation*, Vol. 11, edited by N. Kolesnikov and E. Borisenko (Intech Open Access Publisher, 2012).
- [35] A. Amorese, G. Dellea, L. Braicovich, and G. Ghiringhelli, [arXiv:1410.1587](https://arxiv.org/abs/1410.1587).
- [36] K. Kummer, A. Tamborrino, A. Amorese, M. Minola, L. Braicovich, N. B. Brookes, and G. Ghiringhelli, *J. Synchrotron Radiat.* **24**, 531 (2017).
- [37] P. Wissgott and K. Held, *Eur. Phys. J. B* **89**, 5 (2016).